

On the Vortex Dynamics in the Wake of High-Speed Low-Damping Galloping Cylinders



L. Gan, H. O. Claydon, Q. Y. Wang and S. J. Xu

Abstract In this work, we focus on the vortex evolutions in the wake behind three non-axisymmetric rigid cylinders under high-speed, low-damping galloping in a wind tunnel. Laser displacement sensor is used to measure the displacement amplitude and two branches of amplitude curves are observed—rising and falling range of galloping range. Particle Image Velocimetry is then used to investigate coherent vortex structures in the wake. It has been found that a D-section cylinder has a galloping response at the lowest free stream velocity, which also has the smallest formation length and recirculation bubble length when at static condition. The wake widths show a similar growth rate, which is independent of the galloping amplitudes.

Keywords High-speed galloping · Low-damping · Amplitude spectra
Vortex dynamics · PIV

1 Introduction

Flow induced galloping is a well known phenomenon associated with non-axisymmetric sectional slender bluff-bodies exposed in high velocity cross flows. While there have been extensive experimental studies trying to understand it, most of them either focused on the structure responses or the qualitative vortex patterns (modes) in vortex induced vibration (VIV, happens at lower free stream velocities) regime [1]. In this work, we conduct experimental investigations trying to tackle quantitative vortex evolution in the wake of the galloping non-circular cylinders, aiming for both initial and terminal branches of the amplitude response curves. Our primary interest is the use of the large vibrating amplitude for potential applications in flow mixing and energy harvesting.

L. Gan (✉) · H. O. Claydon
Department of Engineering, Durham University, DH1 3LE, Durham, UK
e-mail: lian.gan@durham.ac.uk

Q. Y. Wang · S. J. Xu
AML, School of Aerospace Engineering, Tsinghua University, Beijing 100084, China

2 Experimental Method and Results

Aluminium cylinders of three cross-sectional shapes are spring mounted horizontally in a wind tunnel (outside) so that the vibration is in the transverse direction; see Fig. 1a. The length/diameter ratio $L/D = 15$, which gives a blockage ratio $\phi = 6\%$ in the wind tunnel so that the flow two-dimensionality is well preserved. The system’s natural frequency f_n and damping ratio ζ are determined from the free oscillation amplitude A_y , measured by a Baumer laser displacement sensor, which operates at 1kHz with a resolution of $50 \mu\text{m}$, and is also used to measure A_y in the galloping states. The system’s natural frequency is given in Table 1 and they result in similar Scruton numbers $Sc \equiv (4\pi m\zeta)/(\rho D^2) \approx 10$, with m being mass per unit length and ρ being the density of air.

The wind tunnel velocity is set at $U_\infty \approx 3 - 15 \text{ m/s}$. The A_y responses are presented in Fig. 1b. We target high reduced speed conditions, i.e. $U_\infty/Df > 20$, where f is the vibration frequency. For the D-section cylinder (DS), $A_y/D > 2.2$ where spring limit is reached at $U_\infty/Df \approx 25$, suggesting the widest response compared to the

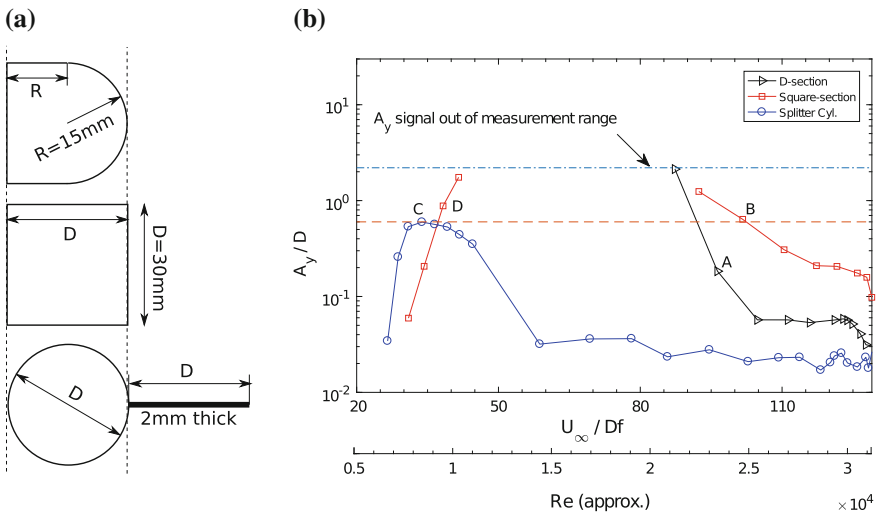


Fig. 1 **a** The cylinder cross sectional shapes; from top to bottom: D-section (DS), square-section (SQ) and Splitter plate-section (SP). The flow comes from the left to the right. **b** Dependence of the oscillation amplitude on the reduced velocity, U_∞ ramps up from low value. The PIV measurement are conducted at the condition near A–D

Table 1 System natural properties

	D-section	Square-section	Splitter plate
f_n (Hz)	3.96	3.74	4.03
$\zeta(\times 10^{-4})$	3.53	3.73	5.65

other two cylinders. Based on the quasi-steady theory, the critical wind speed of galloping is $U_g \equiv 2Scf_n D/a_g$, where $a_g = -dC_L/d\alpha(0) - C_D(0)$. It is well documented in [2, 3] that over a wide testing conditions and cylinder shapes, $-6 \lesssim \alpha_g \lesssim -1$, which gives $0.4 \lesssim U_g \lesssim 2.5$. It has also been shown in [1, 3] that for general bluff bodies in high Re flows, the Strouhal number $St \equiv f_s D/U_\infty \sim 0.1$, where f_s is the vortex shedding frequency, which infers the Kármán-vortex resonance wind speed $U_r \equiv f_n D/St \sim 1$. The ratio $U_g/U_r \lesssim 2.5$ and therefore it indicates that the vibration observed is highly likely a full interaction of VIV and galloping.

Particle Image Velocimetry (PIV) measurements are conducted in the near wake area of $6D \times 7D$ (streamwise), starting from the downstream vertical dashed line in Fig. 1a. PIV images are processed at 32 pixel interrogation window size with 50% overlap, resulting in a spatial resolution of $D/10$ based on vector spacings. PIV measurements are carried out for each cylinder at both static and galloping conditions, which are measured at $U_\infty = 4.5$ and 12 m/s. In total 800 velocity fields are acquired in each case. The testing points at galloping are indicated in Fig. 1b. It has been found from the A_y spectra (figure not shown) that at these testing points, dominant oscillation frequency matches f_n , which is similar to the VIV resonance for large mass ratio structures [1]. The PIV sample rate is set at 3 Hz for all the cases to allow snapshots to be evenly sampled at all phases (vortex shedding and A_y) of a cycle. This is to ensure that all the ensemble averaged process are not phase-locked. The DS A_y spectra also shows more pronounced (compared to SQ) peaks at higher frequencies (not super-harmonics) at a similar reduced velocity, which suggests a multi-scale vortex shedding. Further time resolved measurements will be useful to understand this mechanism.

From the mean velocity field, the development of the wake width defined at half deficit velocity $H[(1/2)(U_\infty - U_0)]$ is shown in Fig. 2. Evidently, the absolute value of H is strongly correlated with A_y , whereas the growth rate is not. Galloping cases tend to have lower growth rates at the same U_∞ for $x > 3D$, which should be attributed to the intensive near-field mixing between the more segmented vortices and regions outside the wake.

Figure 3 presents the relation between the formation length L_f (determined by the peak value of the transverse velocity fluctuations) and the recirculation bubble size (determined by the stagnation point location) B_s . For static cases at $U_\infty = 12$ m/s, L_f and B_s share a similar size for SQ and DS. Noticeable differences can be observed for other cases. For the galloping cases, it is interesting to see that A_y has no strong influence on B_s and L_f ; see the $U_\infty = 12$ m/s cases.

Standard snapshot based proper orthogonal decomposition (POD) is used to track cores of the shed vortices in reduced-order reconstructed vorticity (ω) fields. Subsequently their evolution can be assessed by a conditional average process (not phase averaging). Using DS(F4.5) as an example, Fig. 4a shows a 95% POD energy reconstruction of an instantaneous snapshot (b). The centre of each vortex core in (a) can then be determined after a proper image segmentation process. Comparing Fig. 4a, b, it is not surprising to see that the reduced-order reconstruction shows more organised coherent vortex structures, but the peak ω intensity is lower than that of the true ω . The vortex patterns in the cases shown in Fig. 4 are well pinched-off from the

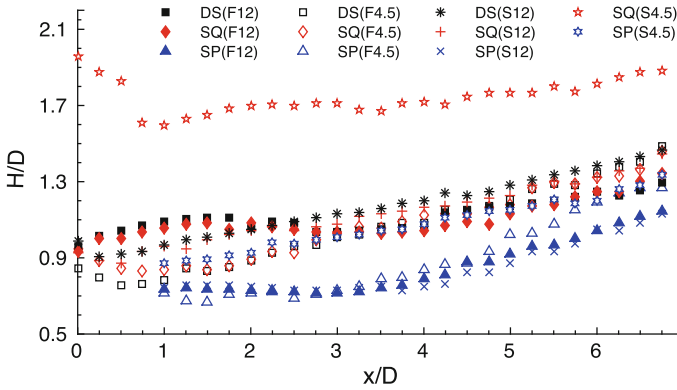


Fig. 2 Development of the wake width H with streamwise distance x . Legend example: DS(F12) stands for static (fixed) DS at $U_\infty = 12$ m/s, SQ(S4.5) for galloping (sprung) SQ at $U_\infty = 4.5$ m/s. This legend system is adopted hereafter

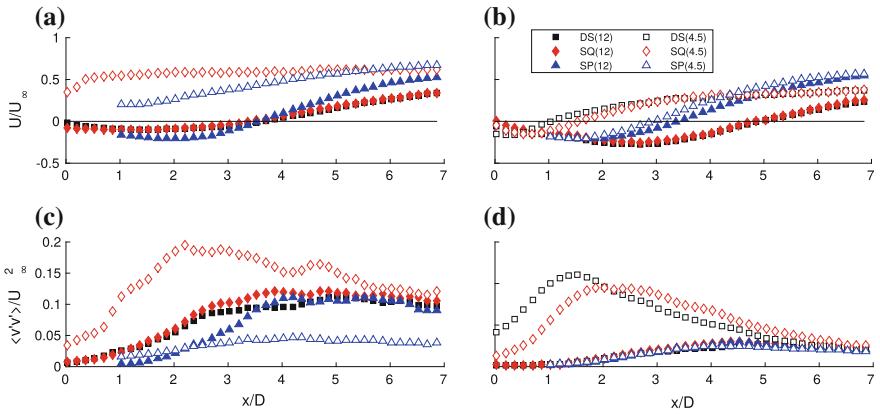


Fig. 3 Recirculation bubble size, defined by the distance of the cylinder centre to the wake stagnation point, which can be determined from the streamwise velocity U along the wake centreline, and formation length, in this case defined by the peak spanwise Reynolds stress $\langle v'v' \rangle$ along the centreline. **a, c** galloping cases; **b, d** static cases. Legends are shown in **(b)**

shear layers. Their strength can be estimated by the approximated circulation Γ_e . Assuming circular vortices, $\Gamma_e = 2\pi \int_0^{R_t} \omega(r)rdr$, where R_t is the radius subjected to a universal threshold or a relative one of $\omega_t = 0.1\omega_0$, with ω_0 being the peak vorticity intensity. The evolution of Γ_e will be presented in a future work, considering the length of the current manuscript.

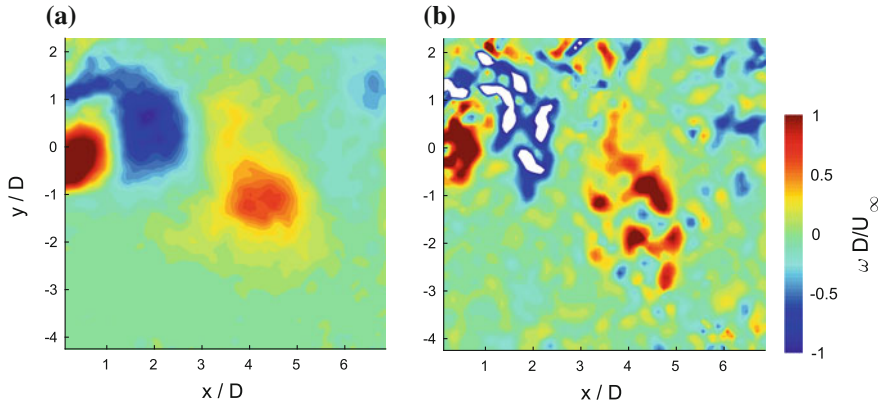


Fig. 4 **a** Reduced-order reconstruction using POD modes of an instantaneous snapshot shown in **b** for DS(F4.5), where **a** contains 95% of the total energy of **b**

3 Conclusion

We present in this paper some wind tunnel measurements of galloping behaviour and wakes behind three non-axisymmetric cylinders. The primary results show that DS has the widest galloping response compared to SQ and SP in terms of amplitude A_y . The PIV measurements reveal that SQ and DS exhibit distinguishable differences in terms of formation length, which is potentially associated with the observed different A_y responses. DS shows to have the smallest formation length and recirculation bubble length in fixed conditions. However, DS and SQ share a similar variation trend for the wake width H at static conditions independently to A_y , with SP having a subtly larger growth rate. The H magnitude is approximately proportional to A_y , not surprisingly.

Acknowledgements The authors thank the support from UK Royal Academy of Engineering (NRCP/1415/130) and China NSFC (11472158).

References

1. Williamson CHK, Govardhan R (2004) Vortex-induced vibrations. *Annu Rev Fluid Mech* 36
2. Wang Q, Song K, Xu S (2015) Experimental study of a spring-mounted wide-D-section cylinder in a cross flow. In: 3rd symposium on fluid-structure-sound interactions and control
3. Mannini C, Marra AM, Bartoli G (2014) VIV galloping instability of rectangular cylinders: review and new experiments. *J Wind Eng Ind Aerodyn* 132